LHCb-CONF-2011-007
March 28, 2011

Improved Measurements of the Cabibbo Favored $B_{(s)} \to D_{(s)}\pi\pi\pi$ and $\Lambda_b \to \Lambda_c\pi\pi\pi$ Branching Fractions

The LHCb Collaboration [1]

Abstract

We report measurements of the branching fractions of the five and six-body decays $X_b \to X_c\pi^-\pi^+\pi^-$ relative to $X_b \to X_c\pi^-$, where X_b (X_c) represents $\bar{B}^0$ (D^+), B^- (D^0), $\bar{B}_s^0$ (D_s^+) and Λ_b^0 (Λ_c^+). The measurements are performed with the LHCb detector using 35 pb^{-1} of data collected at $\sqrt{s} = 7$ TeV. The ratio of branching fractions are measured to be:

$$\frac{\mathcal{B}(\bar{B}^0 \to D^+\pi^-\pi^+\pi^-)}{\mathcal{B}(\bar{B}^0 \to D^+\pi^-)} = 2.35 \pm 0.11(\text{stat}) \pm 0.24(\text{syst})$$
$$\frac{\mathcal{B}(B^- \to D^0\pi^-\pi^+\pi^-)}{\mathcal{B}(B^- \to D^0\pi^-)} = 1.26 \pm 0.07(\text{stat}) \pm 0.12(\text{syst})$$
$$\frac{\mathcal{B}(\bar{B}_s^0 \to D_s^+\pi^-\pi^+\pi^-)}{\mathcal{B}(\bar{B}_s^0 \to D_s^+\pi^-)} = 2.22 \pm 0.41(\text{stat}) \pm 0.25(\text{syst})$$
$$\frac{\mathcal{B}(\Lambda_b^0 \to \Lambda_c^+\pi^-\pi^+\pi^-)}{\mathcal{B}(\Lambda_b^0 \to \Lambda_c^+\pi^-)} = 1.32 \pm 0.15(\text{stat}) \pm 0.14(\text{syst})$$

These measurements are significantly better than or competitive with the world average values.

[1] Conference report prepared for La Thuile 2011, LaThuile, Aosta Valley, Italy; contact author: Steven Blusk

1 Introduction

A core part of the LHCb physics programme is to use $B \to Dh$ decays to overconstrain the parameters of the CKM matrix [1] by performing measurements of mixing and CP violating phenomena. Most generic new physics (NP) models include particles that couple non-trivially to the quark sector, and these new particles, presumably at large mass, can contribute to a number of b decays through virtual loop diagrams. Measuring either directly or indirectly the CKM parameters in processes that have different sensitivities to NP could reveal the presence of new physics, or provide tight constraints on its couplings to the quark sector. One such set of important measurements is the phase of V_{ub} relative to V_{cb}, also referred to as γ or ϕ_3. Direct measurements of γ to date have relied principally on $B^- \to D^* K^{(*)-}$, where the $(b \to c\bar{u}s)$ transition interferes with the $(b \to u\bar{c}s)$ when the D^0 or $\bar{D}^0$ decay to a common final state [2, 3, 4]. Because the b hadron is charged, only integrated signal yields in specific final states are needed. Moreover, this class of decays has only tree-level contributions, and thus it is expected to provide a clean measurement of γ, free from NP contributions. Any deviation in the γ value obtained using decays of this type, from the value inferred from other loop-sensitive observables would be a clear indication for NP. To improve on the current precision on γ that is still above $\sim 10^o$ [5, 6] will require the large statistics expected from LHCb.

In addition to $B^- \to D^* K^{(*)-}$, one can exploit similar interference effects in the decays $B_s^0 \to D_s^{\pm} K^{\mp}$ and $\bar{B}_s^0 \to D_s^{\mp} K^{\pm}$. Unlike the B^- decay, here the B_s^0 mesons oscillate, and one must perform a time-dependent analysis. Another mode of interest is $\bar{B}^0 \to D^+\pi^-$. Here, access to γ is enabled by the interference between the direct $b \to c\bar{u}d$ decay and one with mixing followed by decay, *e.g.* $b \to \bar{b} \to \bar{u}c\bar{d}$.

To obtain the most precise measurement of γ with a finite data sample, all of these methods (and others) will be pursued. Three such additional decay modes that may be useful for the γ measurement are the decays $B^- \to D^0 K^-\pi^+\pi^-$, $\bar{B}^0 \to D^+\pi^-\pi^+\pi^-$, and $\bar{B}_s^0 \to D_s^+ K^-\pi^+\pi^-$. These decays are quite similar to $B^- \to D^0 K^-$, $\bar{B}^0 \to D^+\pi^-$, and $B_s^0 \to D_s^{\mp} K^{\pm}$, respectively, the difference being that the $s\bar{u}$ ($d\bar{u}$) fragments into a $K^-\pi^+\pi^-$ ($\pi^-\pi^+\pi^-$), instead of a K^- (π^-) [$D^{*(*)}\pi(\pi)$ are also included.] The advantage of these decays are that their branching fractions are expected to be significantly larger, thus potentially providing additional statistics for the γ measurement. If the $K^-\pi^+\pi^-$ or $\pi^-\pi^+\pi^-$ are dominated by a single resonance, then the same formalism for extracting γ using $B_{(s)} \to D_{(s)}h$ applies to these decays as well. If not, one must either model the contributing resonances, or fit for an additional parameter related to the average strong phase shift over the Dalitz plot.

The work presented here represents an exploratory study of the decays, $X_b \to X_c\pi\pi\pi$, with the aim of establishing the rates for these decays. The current precision on these branching fractions is quite poor. The world average values for these decays, and the normalizing modes, $X_b \to X_c\pi^-$, are shown in Table 1.

Because of the similar signatures of these decays, we seek to measure all four of the $X_b \to X_c\pi^-\pi^+\pi^-$ decay modes listed in Table 1, although not all are directly relevant for CP violation studies. The $\bar{B}_s^0 \to D_s^+\pi^-\pi^+\pi^-$ decay is not only useful for measurement of

Table 1: Summary of world average branching fractions measurements for modes used in this analysis [7].

Decay	$\mathcal{B}$ (10^{-3})	$\frac{\mathcal{B}(B\to D+3h)}{\mathcal{B}(B\to Dh)}$
$\bar{B}^0 \to D^+\pi^-\pi^+\pi^-$	8.0 ± 2.5	3.0 ± 0.9
$B^- \to D^0\pi^-\pi^+\pi^-$	11 ± 4	2.3 ± 0.8
$B_s^0 \to D_s^+\pi^-\pi^+\pi^-$	8.4 ± 3.3	2.6 ± 1.1
$\Lambda_b^0 \to \Lambda_c^+\pi^-\pi^+\pi^-$	-	-
$B^0 \to D^+\pi^-$	2.68 ± 0.13	-
$B^- \to D^0\pi^-$	4.84 ± 0.15	-
$\bar{B}_s^0 \to D_s^+\pi^-$	3.2 ± 0.5	-
$\Lambda_b^0 \to \Lambda_c^+\pi^-$	8.8 ± 3.2	-

Δm_s, but provides a direct calibration of the mistag rate needed for the γ measurement using $\bar{B}_s^0 \to D_s^+ K^-\pi^+\pi^-$. The $\Lambda_b^0 \to \Lambda_c^+\pi^-\pi^+\pi^-$ decay is not directly used in CP violation studies, but would be useful to improve knowledge of hadronic Λ_b^0 decays.

2 Experiment and Data Samples

The data used for this analysis comprises 35 pb^{-1} of pp collisions at $\sqrt{s} = 7$ TeV collected by the LHCb experiment during the 2010 data taking period. LHCb has excellent hadron identification capabilities to trigger on and reconstruct bottom and charm hadrons, as well as other specific decays that may signal the presence of NP. The LHCb detector includes a charged particle tracking system that covers the forward angular region from about ± 350 mrad in x and ± 250 mrad in y. It includes a 21-station, one-meter long array of silicon strip detectors (VELO) that come within 8 mm of the LHC beams, a 4 Tm dipole magnetic field, followed by three multi-layer tracking stations downstream of the dipole magnet. Each downstream tracking station is composed of a four-layer silicon strip detector in the high occupancy region near the beam pipe (IT), and an 8-layer straw tube drift chamber composed of 5 mm straws outside this high occupancy region. At the upstream end of the dipole magnet is a four-layer silicon strip detector (TT) that provides about 20-30% relative improvement in the momentum resolution (depending on momentum). Overall, the tracking system provides an impact parameter (IP) resolution of $\sim 16\mu\text{m} + 30\mu\text{m}/p_T$ (p_T in GeV/c), and a momentum resolution that ranges from $\sigma_p/p \sim 0.5\%$ at 3 GeV/c and to $\sim 0.8\%$ at 100 GeV/c. Two Ring Imaging Cherenkov Counters, one upstream of the magnet between VELO and TT (RICH1), and a second just downstream of the tracking stations (RICH2), are used together and provide a typical kaon efficiency of $\sim$95% for a pion fake rate of a few percent, integrated over the momentum range from 3-100 GeV/c. Downstream of RICH2 is a Preshower/Scintillating Pad Detector (PS/SPD), an electromagnetic calorimeter (ECAL), and a hadronic calorimeter (HCAL). The ECAL provides for reconstruction of photons, π^0, and η mesons, and is used

in electron identification. Information from the ECAL/HCAL is also used to form the L0 Hadron triggers. The LHCb detector also features a large, five station muon system. Four of the stations are downstream of the HCAL, and the first is located just upstream of the PS/SPD. A more detailed description of the LHCb detector can be found in the references [8].

To reduce the 40 MHz crossing rate down to 2 kHz of stored events, LHCb uses a two-level trigger system. The first level of the trigger, L0, searches for either a large E_T cluster ($E_T > 3.6$ GeV) in the calorimeters, or a single high p_T or di-muon pair in the muon stations. Events passing L0 are read out into a large computing farm and are analyzed using a software-based trigger. The first level of the software trigger, called HLT1, uses fast versions of the offline software to apply tighter selections on charged particles based on their p_T and minimal IP to any primary vertex (PV)[2]. Several of the lines in HLT1 look to confirm the L0 object, and then apply these tighter selections to the L0 candidate. Another HLT1 line, called the HLT1 OneTrack [9] line, ignores the L0 information and searches for a single track with IP larger than 125 μm, $p_T > 1.25$ GeV/c, $p > 12.5$ GeV/c, along with other track quality requirements. Similar but softer cuts are applied if the track is identified as a muon. Such tracks are quite rare in minimum bias events, and thus large background suppression is achieved. Relative to L0, HLT1 provides an additional suppression of about 20-30 of the minimum bias background. Events that pass HLT1 are analyzed by a second-software level, HLT2, where a trigger based on topological information [10] searches for evidence of b decay vertices. Tracks that have $p > 5$ GeV/c, $p_T > 0.5$ GeV/c and IP χ^2 larger than 16 are used to search for 2, 3 or 4-track vertices consistent with a b-hadron decay. The decay vertex is required to have at least one track with $p_T > 1.5$ GeV/c, a scalar p_T sum of at least 4 GeV/c, and a corrected mass[3] between 4 and 7 GeV/c^2. Other track and vertex quality cuts are applied as well. HLT2 has an efficiency of 80-90% relative to events that pass typical offline selections for a large range of B decays. Other HLT2 triggers also run in parallel to the topological trigger, but are not directly relevant to the analyses presented here.

LHCb was designed to operate at 0.4 interactions/crossing, which gives mostly single pp interactions. For much of the 2010 running, to maximize the integrated luminosity, LHCb operated with in excess of 2 interactions per crossing on average. Very large events are known to have intrinsically high backgrounds and to be slow to reconstruct. Therefore such events were suppressed by applying global event cuts (GECs) to hadronically triggered decays. These GECs included a maximum of 3000 VELO clusters, 3000 IT hits, and 10,000 OT hits. In addition, hadron triggers were required to have less than 900 or 450 hits in the SPD, depending on the specific trigger setting (most of the data was taken with the looser requirement.)

[2]Primary vertices refer to the locations of the reconstructed pp collisions.

[3]The corrected mass is defined as $M_{\rm cor} = \sqrt{M^2 + p^2_{\rm trans}}$, where M is the invariant mass of the 2, 3 or 4-track candidate (assuming the kaon mass for each particle), and $p_{\rm trans}$ is the momentum imbalance transverse to the direction of flight, defined by the vector that joins the primary and secondary vertices.

3 Candidate Reconstruction and Selection

After events are reconstructed, they are *stripped* using loose selection requirements on the decay channels of interest. Tighter offline selections are applied at the analysis stage. Here, we briefly discuss only the most important final analysis selections.

We first identify charged particles that are likely to come from b hadron decays by filtering off those particles that have a minimum IP $\chi^2 > 9$ with respect to any primary vertex (PV), have $p > 2$ GeV/c, and $p_T > 300$ MeV/c [4]. Hadrons are identified by requiring the difference in log-likelihoods of the different mass hypotheses to satisfy $\Delta LL(K-\pi) > -5$, $\Delta LL(p-\pi) > -5$ and $\Delta LL(K-\pi) < 12$, for kaons, protons and pions, respectively. These particle lists are not exclusive, but any given particle can only be used once in forming multi-body decays.

Charm particle candidates are reconstructed in the decay modes $D^0 \to K^-\pi^+$, $D^+ \to K^-\pi^+\pi^+$, $D_s^+ \to K^+K^-\pi^+$ and $\Lambda_c^+ \to pK^-\pi^+$. A potentially large source of background from prompt charm is suppressed by requiring the charm particle's momentum vector to have a three-dimensional impact parameter (IP3D) and IP3D χ^2 that satisfies IP3D$>$ 0.08 mm and IP3D $\chi^2 > 12.25$. We also require the charm particle candidate to have a minimal flight distance, FD > 2 mm and FD $\chi^2 > 49$. Additional suppression of combinatorial background is provided by requiring $p_T^{X_c} > 1.25$ GeV/c (1.5 GeV/c for $X_b \to X_c\pi^-$). Backgrounds from vertices formed from poorly measured prompt tracks are suppressed by requiring the charm vertex be well displaced transversely from the associated PV ($\Delta R = \sqrt{(\Delta x)^2 + (\Delta y)^2} > 0.1$ mm) and that the χ^2/dof of the vertex fit is less than 8. Lastly, we require the charm particle's mass to be within 25 MeV/c^2 of the known value. A similar set of selection requirements are applied to the $3h$ vertex, except we only require $p_T > 1$ GeV/c and the mass window covers the invariant mass range from 0.8 GeV/$c^2 < M(\pi\pi\pi) <$ 3.0 GeV/c^2.

Beauty hadrons are formed by combining a charm particle with either a single pion candidate (for $X_b \to X_c\pi^-$), or a $3h$ *particle* (for $X_b \to X_c\pi^-\pi^+\pi^-$.) A minimum $p_T >$ 1 GeV/c is required. We also require the b hadron have a minimum IP and IP χ^2 with respect to any PV of less than 90 μm and 16, respectively. To minimize combinatorial background from prompt tracks, we require the b candidate vertex has a FD$>$2 mm, FD $\chi^2 > 49$, and a vertex fit $\chi^2/dof < 6$ (8 for $X_b \to X_c\pi^-$.) We also require that the angle θ between the b-hadron momentum and the vector formed by joining the PV and decay vertex is such that $\cos\theta > 0.99996$. Lastly to suppress potentially low multiplicity primary vertices contributing background, we require that the candidate b-hadron decay vertex be displaced by more than 100 μm transversely from the associated PV.

In addition to these selections, to control the timing to process very busy events, the $X_b \to X_c\pi^-$ stripping line includes additional requirements on the maximum number of long tracks[5] in an event. For $\bar{B}^0 \to D^+\pi^-$ and $\bar{B}_s^0 \to D_s^+\pi^-$, the maximum number of long tracks is 180, and for $\Lambda_b^0 \to \Lambda_c^+\pi^-$ and $B^- \to D^0\pi^-$ it is 120. These selections are

[4] For the $B \to D + 3h$ decays, we allow at most one track to have 200 MeV/$c < p_T <$ 300 MeV/c.

[5] Long tracks refer to charged particles that have segments in both the VELO and the T-stations, and thus have the nominal $\sigma_p/p \sim 0.5\%$.

99% and 95% efficient, respectively, after the GECs. The $X_b \to X_c\pi^-\pi^+\pi^-$ requires fewer than 300 long tracks, and thus is essentially 100% efficient after the GECs.

Lastly, we note that in $X_b \to X_c\pi^-\pi^+\pi^-$, between 4% and 10% of events have multiple candidates (mostly two). In such cases we choose the candidate with the largest p_T. This selection is estimated to be $(75 \pm 20)\%$ efficient in choosing the correct candidate. For $X_b \to X_c\pi^-$ multiple candidates occur in less than 1% of events, from which we again choose the one with the largest p_T. The inclusion of charge conjugate final decays is implied.

4 MC Simulation and Selection Efficiency

Monte Carlo (MC) samples are generated to evaluate both selection and trigger efficiencies. The data are simulated with an average number of interactions per crossing equal to 2.5, which is similar to the running conditions for the majority of the 2010 data. The b-hadrons are produced using PYTHIA [11], which includes the contributions from all expected production mechanisms, such as gluon fusion, flavour excitation, and gluon-splitting, along with smaller contributions from other processes. Once produced, the b hadrons are decayed using EVTGEN [12]. The $X_b \to X_c\pi^-$ decays are produced flat in phase space. The $X_b \to X_c\pi^-\pi^+\pi^-$ are simulated using a cocktail for the $\pi\pi\pi$ that is $\sim$2/3 $a_1(1260)^-$ and about 1/3 $\rho^0\pi^-$ (non-resonant). Smaller contributions from $D_1^0(2420)\pi^-$ and $D_2^{*0}(2460)\pi^-$ each contribute at the 5% level to $B^- \to D^0\pi^-\pi^+\pi^-$. For $\Lambda_b^0 \to \Lambda_c^+\pi^-\pi^+\pi^-$, we include contributions from $\Lambda_c(2595)^+$ and $\Lambda_c(2625)^+$, which comprise about 16% of the rate. The response of the detector to the final state particles is simulated with GEANT [13], and also includes additional tunings to model various detector responses, dead channels, spillover, and other electronic effects. The digitized output is passed through the standard offline reconstruction, including the trigger simulation and the stripping, and throughout is reconstructed in the same way as real data.

Using the simulation, we evaluate the total efficiency for each decay to pass all selection and trigger requirements. The contributions to the total efficiency are subdivided into several *sub-efficiencies*, as shown in Table 2. The first efficiency, $\epsilon_{\rm geo}$ is a geometrical efficiency for all stable daughter particles from the X_b decay to be in the angular range from 10-400 mrad; $\epsilon_{\rm det}/\epsilon_{\rm geo}$ is the fraction of those decays in which all daughters are reconstructible as long tracks; $\epsilon_{\rm trk}/\epsilon_{\rm det}$ is the efficiency of reconstructing all the B daughter tracks as long tracks given that they were reconstructible as such; and $\epsilon_{\rm sel}/\epsilon_{\rm trk}$ is the total selection efficiency resulting from the various signal selection requirements. The kinematic efficiency, $\epsilon_{\rm kin}$ is the product of all the previous efficiency components. The total kinematic efficiency ranges from about 0.11% to 1.5%.

The second component of the efficiency is the trigger efficiency. In order to have a well-defined trigger path, all decays are required to satisfy the L0 Hadron trigger, the HLT1 OneTrack line, and a logical OR of the HLT2 Topological (2, 3, 4)-body trigger lines. Here, we specifically require that at least one of the X_b hadron's daughters coincide with the L0 and HLT1 objects that gave rise to these triggers. The efficiencies of the

Table 2: Summary of efficiencies as determined from MC simulation for decay channels under study, as described in the text. The geometric efficiencies are the fraction of b hadrons produced within 400 mrad of the $+z$-axis. † For these samples, the geometric efficiency also includes the requirement that the (charged) b-hadron daughters have polar angles between 10 and 400 mrad.

Decay	$\epsilon_{\rm geo}$ (%)	$\epsilon_{\rm det}/\epsilon_{\rm geo}$ (%)	$\epsilon_{\rm trk}/\epsilon_{\rm det}$ (%)	$\epsilon_{\rm sel}/\epsilon_{\rm trk}$ (%)	$\epsilon_{\rm kin}$ (%)
$B^0 \to D^+\pi^-\pi^+\pi^{-\dagger}$	13.6 ± 0.1	10.8 ± 0.1	84.9 ± 0.3	12.3 ± 0.2	0.153 ± 0.003
$B^- \to D^0\pi^-\pi^+\pi^{-\dagger}$	14.2 ± 0.1	15.7 ± 0.1	87.5 ± 0.3	14.1 ± 0.3	0.275 ± 0.007
$B_s^0 \to D_s^+\pi^-\pi^+\pi^{-\dagger}$	14.5 ± 0.1	10.4 ± 0.1	85.3 ± 0.2	10.6 ± 0.2	0.136 ± 0.003
$\Lambda_b^0 \to \Lambda_c^+\pi^-\pi^+\pi^{-\dagger}$	14.3 ± 0.1	10.3 ± 0.1	82.3 ± 0.2	9.1 ± 0.4	0.111 ± 0.005
$B^0 \to D^+\pi^{-\dagger}$	15.3 ± 0.2	24.8 ± 0.1	90.7 ± 0.2	25.6 ± 0.2	0.885 ± 0.014
$B^- \to D^0\pi^-$	32.7 ± 0.3	16.5 ± 0.1	94.0 ± 0.1	30.3 ± 0.2	1.53 ± 0.02
$B_s^0 \to D_s^+\pi^{-\dagger}$	16.1 ± 0.1	23.8 ± 0.1	91.8 ± 0.1	24.7 ± 0.2	0.869 ± 0.010
$\Lambda_b^0 \to \Lambda_c^+\pi^-$	34.0 ± 0.4	11.6 ± 0.1	89.8 ± 0.2	20.7 ± 0.3	0.732 ± 0.015

various triggers are given in Table 3. We see that the L0 efficiency is typically around 35%, whereas HLT1 and HLT2 have efficiencies in the 80-90% range. From the total triggered event sample, 40-50% of the candidates pass all three trigger lines.

Table 3: Summary of trigger efficiencies as determined from MC simulation for decay channels under study, as described in the text.

Decay	$\epsilon_{\rm L0}/\epsilon_{\rm sel}$ (%)	$\epsilon_{\rm HLT1}/\epsilon_{\rm L0}$ (%)	$\epsilon_{\rm HLT2}/\epsilon_{\rm HLT1}$ (%)	$\epsilon_{\rm trig}$ (%)
$\bar{B}^0 \to D^+\pi^-\pi^+\pi^-$	32.1 ± 0.6	82.0 ± 0.9	86.0 ± 0.9	22.6 ± 0.5
$B^- \to D^0\pi^-\pi^+\pi^-$	36.9 ± 0.7	83.3 ± 0.8	89.1 ± 0.8	27.4 ± 0.6
$\bar{B}_s^0 \to D_s^+\pi^-\pi^+\pi^-$	34.1 ± 0.7	81.4 ± 1.4	89.7 ± 1.2	24.9 ± 0.7
$\Lambda_b^0 \to \Lambda_c^+\pi^-\pi^+\pi^-$	32.2 ± 0.8	81.1 ± 1.1	91.8 ± 0.9	24.0 ± 0.7
$\bar{B}^0 \to D^+\pi^-$	31.7 ± 0.3	82.7 ± 0.4	79.4 ± 0.5	20.8 ± 0.3
$B^- \to D^0\pi^-$	37.5 ± 0.3	86.1 ± 0.4	85.0 ± 0.4	27.4 ± 0.3
$\bar{B}_s^0 \to D_s^+\pi^-$	32.1 ± 0.2	82.0 ± 0.6	87.9 ± 0.2	23.1 ± 0.2
$\Lambda_b^0 \to \Lambda_c^+\pi^-$	32.1 ± 0.4	84.0 ± 0.6	91.5 ± 0.5	24.7 ± 0.4

We have also checked that the acceptance is flat across $M(\pi\pi\pi)$, both after analysis selection and after applying the full trigger selection to simulated events. A fit to the efficiency over the range from 0.8-3 GeV yields slopes of $(0.25 \pm 0.33)\%$ $[(-0.14 \pm 0.14)\%]$ per GeV for the offline-selection [offline-selected and triggered] event sample.

5 Reconstructed Signals in Data

The reconstructed $X_b \to X_c\pi^-\pi^+\pi^-$ invariant mass distributions after the full offline and trigger selection are shown in Fig. 1. From top left to bottom right are shown $\bar{B}^0 \to D^+\pi^-\pi^+\pi^-$, $B^- \to D^0\pi^-\pi^+\pi^-$, $\bar{B}^0_s \to D^+_s\pi^-\pi^+\pi^-$, and $\Lambda^0_b \to \Lambda^+_c\pi^-\pi^+\pi^-$. Unbinned maximum-likelihood fits are performed, with likelihood functions given by the sums of signal and several background components. The signal and background components are shown in the figures. The signal shapes are each parameterized by a double Gaussian with equal means. We constrain the fractional area in the narrower (core) Gaussian and the ratio of the wider to narrower Gaussian widths using signal MC. The core width is allowed to float, as the absolute resolution in data is larger than in the simulation. For $\bar{B}^0_s \to D^+_s\pi^-$ and $\bar{B}^0_s \to D^+_s\pi^-\pi^+\pi^-$, we also constrain the core Gaussian widths based on the resolutions found in data for the kinematically similar decays $\bar{B}^0 \to D^+\pi^-$ and $\bar{B}^0 \to D^+\pi^-\pi^+\pi^-$, respectively, scaled by 0.93, which is the ratio of widths obtained from MC simulation. A number of backgrounds contribute to these decays. Below the b hadron masses there are generally peaking background structures due to $B_{(s)} \to D^*_{(s)}\pi\pi\pi$, with a missed photon, π^0 or π^+. For the $\bar{B}^0$ and B^- decays, shapes of these backgrounds are taken from signal MC simulations; the relative fractions are allowed to float. There is a small contamination from Cabibbo-suppressed decays, which, due to the $\tan^2\theta_C$[6] suppression and the excellent RICH performance are limited to be $(1 \pm 1)\%$ of the signal yield. For B^0_s, the low mass peaking background shape is derived from a large inclusive $b \to D^+_s X$ Monte Carlo sample. For the Λ^0_b, very few decays modes are measured, and there does not appear to be any peaking structures in the background, so we do not include any low mass peaking backgrounds. The combinatorial background is modeled with an exponential in all cases.

There are also non-negligible cross-feeds from the $\bar{B}^0 \to D^+\pi^-\pi^+\pi^-$ into $\bar{B}^0_s \to D^+_s\pi^-\pi^+\pi^-$, as well as cross-feed between $\bar{B}^0_s \to D^+_s\pi^-\pi^+\pi^-$ and $\Lambda^0_b \to \Lambda^+_c\pi^-\pi^+\pi^-$. Other cross-feeds are well below the percent level and are negligible. The cross-feed generally occurs when one of the charm hadron daughters is misidentified, and the shifted mass falls within the mass window of another charm hadron. The most important such background is the misidentification of a π^+ as a K^+ in $D^+ \to K^-\pi^+\pi^+$. If the resulting $K^-K^+\pi^+$ mass is within 25 MeV/c^2 of the D^+_s mass, a peaking background is generated in the $\bar{B}^0_s \to D^+_s\pi^-\pi^+\pi^-$ mass spectrum. To estimate this, and other cross-feeds between the various b species, we use a combination of data and MC simulation. For the MC studies, we run the analysis selections for each signal decay on the MC samples from the other $X_b \to X_c\pi^-\pi^+\pi^-$ decay modes. The cross-feed rate is then the fraction of events that are accepted into the incorrect $X_b \to X_c\pi^-\pi^+\pi^-$ decay mode relative to the correct one. For data, we select signal candidates within 50 MeV/c^2 of the signal peak of each $X_b \to X_c\pi^-\pi^+\pi^-$ decay, apply the particle ID (PID) associated with each of the other decay modes, re-assign particle masses based on this PID, apply the charm-hadron mass window requirements of those other selections, and count how many events are reflected

[6] Here, θ_C is the Cabibbo angle.

into the other decay modes. The same procedure is applied to candidates in the B mass sidebands ($60\ \mathrm{MeV}/c^2 < |M - m_B| < 110\ \mathrm{MeV}/c^2$), and this yield is subtracted from that found when using the B signal region. In general the simulation and data give similar results for the cross-feeds, so the absolute rate is taken as the average, and the uncertainty is set to either the difference between the data and MC, or 20% (relative), whichever is larger.

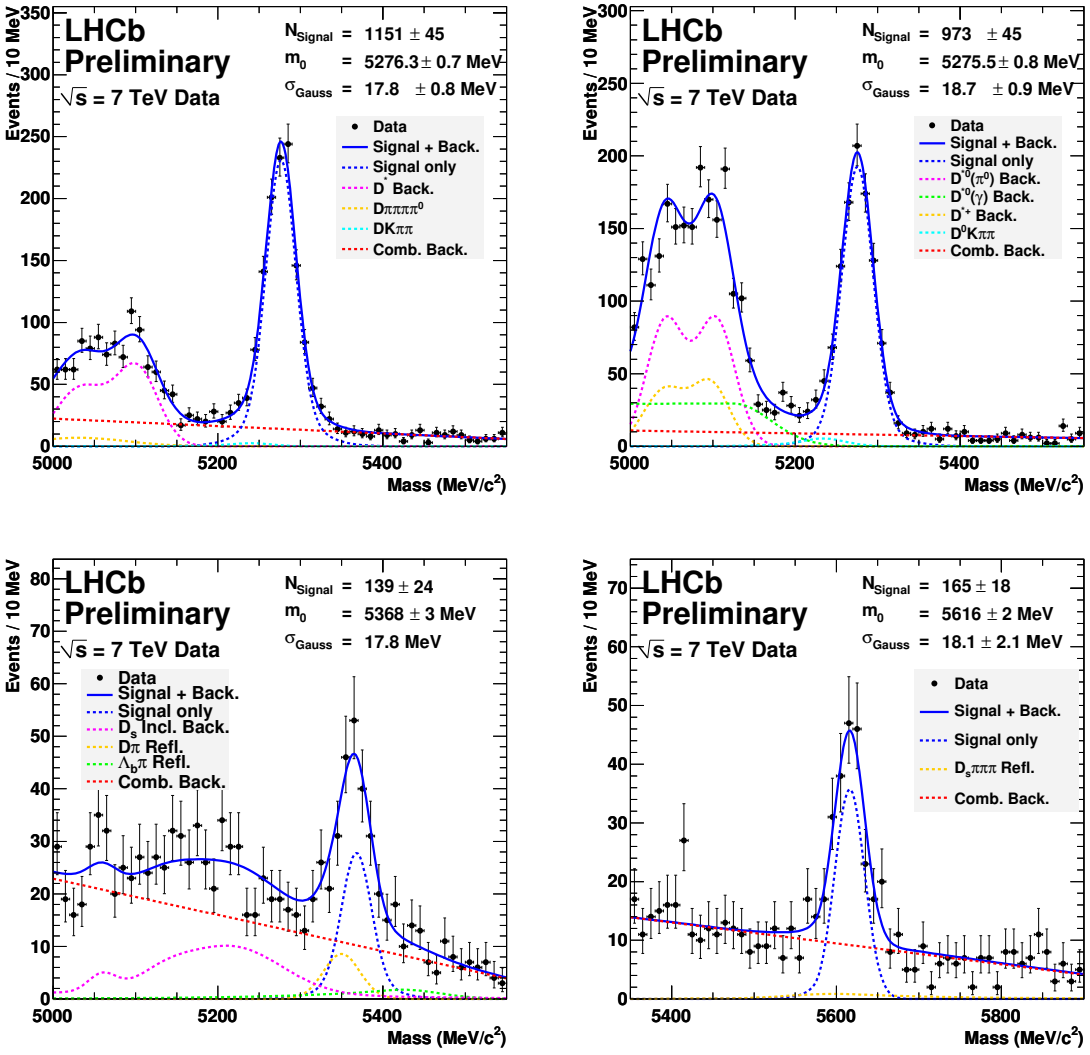

Figure 1: Invariant mass distributions for $\bar{B}^0 \to D^+\pi^-\pi^+\pi^-$ (top left), $B^- \to D^0\pi^-\pi^+\pi^-$ (top right), $\bar{B}^0_s \to D^+_s\pi^-\pi^+\pi^-$ (bottom left), and $\Lambda^0_b \to \Lambda^+_c\pi^-\pi^+\pi^-$ (bottom right). Fits showing the signal and background components are indicated, and are described in the text.

The invariant mass distributions for the normalization modes are shown in Fig. 2. The peaking backgrounds and cross-feed issues are quite similar for $X_b \to X_c\pi^-\pi^+\pi^-$,

and are evaluated in an analogous manner. One additional background to $X_b \to X_c\pi^-$ is the decay $X_b \to X_c\rho^+$, which is included in the B^- and $\bar{B}^0$ likelihood fits. For the B_s^0, we use the inclusive signal MC, as described above and for $\Lambda_b^0 \to \Lambda_c^+\pi^-$, we use a Gaussian model to describe the low mass excess, which will include contributions from $\Lambda_b^0 \to \Lambda_c^-\rho^+$, $\Lambda_b^0 \to \Sigma_c^+\pi^- \to \Lambda_c^+\pi^0\pi^-$, and other decays. The signal yields are summarized in Table 4.

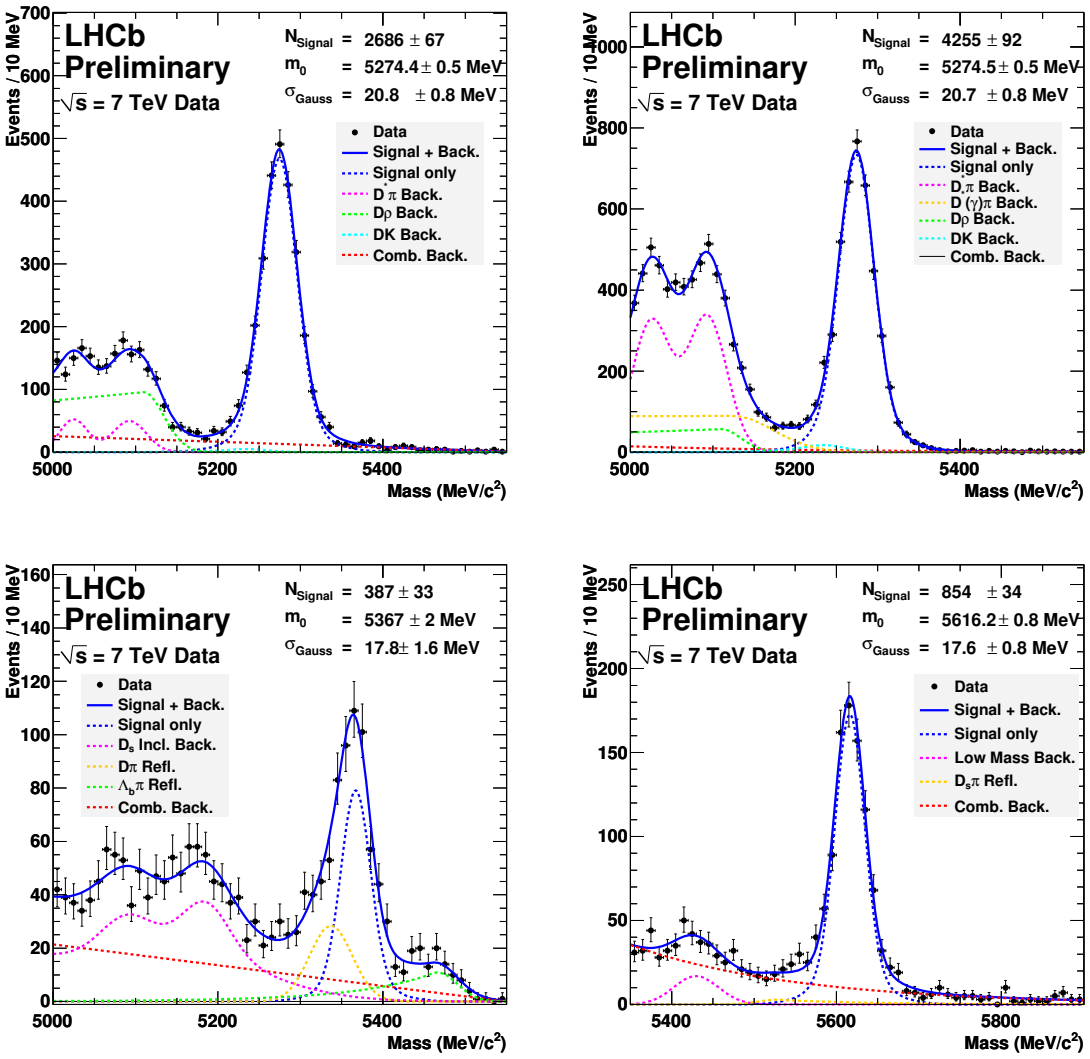

Figure 2: Invariant mass distributions for $\bar{B}^0 \to D^+\pi^-$ (top left), $B^- \to D^0\pi^-$ (top right), $\bar{B}_s^0 \to D_s^+\pi^-$ (bottom left), and $\Lambda_b^0 \to \Lambda_c^+\pi^-$ (bottom right). Fits showing the signal and background components are indicated, and are described in the text.

6 Substructures in the $X_b \to X_c\pi^-\pi^+\pi^-$

To confirm our expectation that the $X_b \to X_c\pi^-\pi^+\pi^-$ decays predominantly through $X_b \to X_c a_1(1260)^+ \to X_c\pi\pi\pi$, we show in Fig 3 the sideband-subtracted $\pi\pi\pi$ invariant mass for each of the four decay modes. The points are the sideband subtracted data and the solid line is the simulation. The simulation is comprised of about 2/3 $a_1(1260)^+$, and about 1/3 non-resonant $\rho^0\pi^+$. To increase statistics in $\bar{B}^0_s \to D^+_s\pi^-\pi^+\pi^-$ and $\Lambda^0_b \to \Lambda^+_c\pi^-\pi^+\pi^-$ these plots include all signal decays, as opposed to just those that are accepted by our specific trigger lines.) We observe structure that is consistent with what one would expect from the $a_1(1260)^+$ in all four decay modes. We find that our 3π mass spectrum appears to be shifted toward lower mass as compared to the MC simulation. However, the world average $a_1(1260)^+$ mass is (1230 ± 40) MeV/c^2 [7], and may be process-dependent, so it is difficult to draw any definitive conclusion from this shift in mass. Because our reconstruction and trigger efficiency are flat in $M(\pi\pi\pi)$, this shift does not introduce any bias in the detection efficiencies.

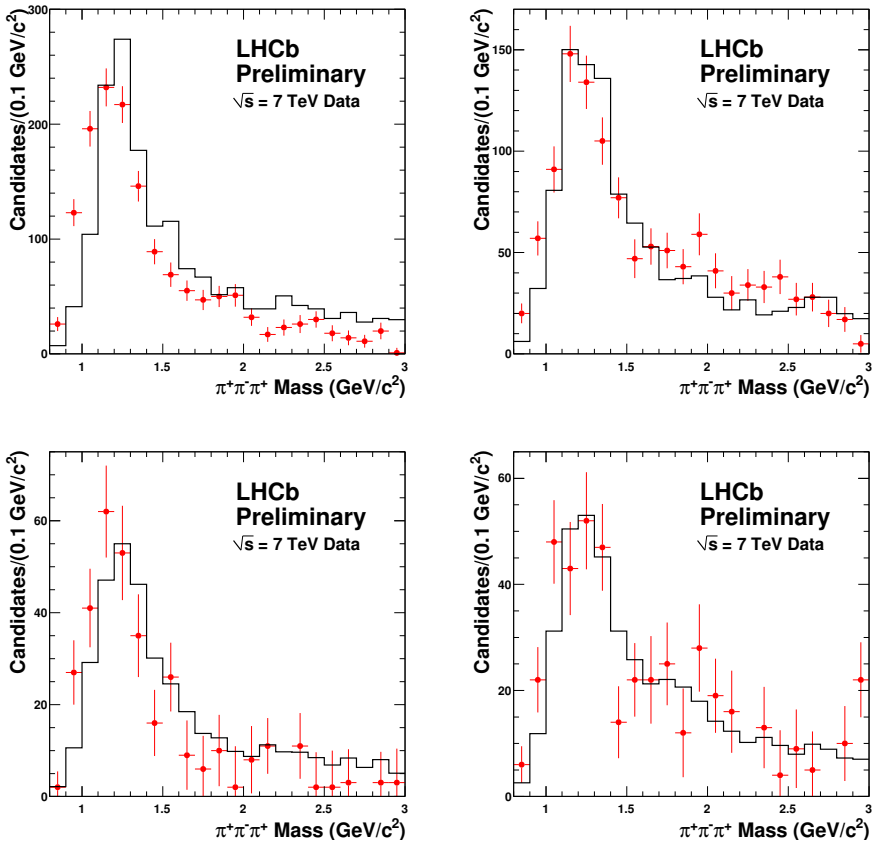

Figure 3: Invariant mass of the 3π bachelor in $\bar{B}^0 \to D^+\pi^-\pi^+\pi^-$ (top left), $B^- \to D^0\pi^-\pi^+\pi^-$ (top right), $\bar{B}^0_s \to D^+_s\pi^-\pi^+\pi^-$ (bottom left) and $\Lambda^0_b \to \Lambda^+_c\pi^-\pi^+\pi^-$ (bottom right) decays. The data are the points with error bars and the simulation is the solid line.

7 Branching fraction results

The ratio of branching ratios is computed using:

$$\frac{\mathcal{B}(X_b \to X_c\pi^-\pi^+\pi^-)}{\mathcal{B}(X_b \to X_c\pi^-)} = \frac{Y(X_b \to X_c\pi^-\pi^+\pi^-)}{Y(X_b \to X_c\pi^-)} \frac{\epsilon_{\rm kin}(X_b \to X_c\pi^-)}{\epsilon_{\rm kin}(X_b \to X_c\pi^-\pi^+\pi^-)} \frac{\epsilon_{\rm trig}(X_b \to X_c\pi^-)}{\epsilon_{\rm trig}(X_b \to X_c\pi^-\pi^+\pi^-)}$$

where Y are the observed yields, and $\epsilon_{\rm kin}$ and $\epsilon_{\rm trig}$ are the kinematic and trigger efficiencies. The relevant input numbers are shown in Table 4.

Table 4: Summary of inputs for the branching fraction computation. Uncertainties are statistical only.

Decay	Yield	ϵ_{kin} (%)	ϵ_{trig} (%)
$\bar{B}^0 \to D^+\pi^-\pi^+\pi^-$	1151 ± 45	0.153 ± 0.003	22.6 ± 0.5
$B^- \to D^0\pi^-\pi^+\pi^-$	973 ± 45	0.275 ± 0.007	27.4 ± 0.6
$\bar{B}^0_s \to D^+_s\pi^-\pi^+\pi^-$	139 ± 24	0.136 ± 0.003	24.9 ± 0.7
$\Lambda^0_b \to \Lambda^+_c\pi^-\pi^+\pi^-$	165 ± 18	0.111 ± 0.005	24.0 ± 0.7
$\bar{B}^0 \to D^+\pi^-$	2686 ± 67	0.885 ± 0.014	20.8 ± 0.3
$B^- \to D^0\pi^-$	4255 ± 92	1.53 ± 0.02	27.4 ± 0.3
$\bar{B}^0_s \to D^+_s\pi^-$	387 ± 33	0.869 ± 0.010	23.1 ± 0.2
$\Lambda^0_b \to \Lambda^+_c\pi^-$	887 ± 38	0.732 ± 0.015	24.7 ± 0.4

The uncorrected ratios of branching fractions are:

$$\frac{\mathcal{B}(\bar{B}^0 \to D^+\pi^-\pi^+\pi^-)}{\mathcal{B}(\bar{B}^0 \to D^+\pi^-)} = 2.27 \pm 0.11(\text{stat})$$
$$\frac{\mathcal{B}(B^- \to D^0\pi^-\pi^+\pi^-)}{\mathcal{B}(B^- \to D^0\pi^-)} = 1.28 \pm 0.07(\text{stat})$$
$$\frac{\mathcal{B}(\bar{B}^0_s \to D^+_s\pi^-\pi^+\pi^-)}{\mathcal{B}(\bar{B}^0_s \to D^+_s\pi^-)} = 2.13 \pm 0.41(\text{stat})$$
$$\frac{\mathcal{B}(\Lambda^0_b \to \Lambda^+_c\pi^-\pi^+\pi^-)}{\mathcal{B}(\Lambda^0_b \to \Lambda^+_c\pi^-)} = 1.32 \pm 0.15(\text{stat})$$

8 Systematics Uncertainties

Several sources of systematic uncertainty that enter into this analysis are described in this section, and are summarized in Table 5.

The tracking efficiency systematic uncertainty is estimated to be 3% [14] based on the ratio of corrected yields for $B \to D^0 X \mu^+ \nu,\ D^0 \to K\pi\pi\pi$ to $B \to D^0 X \mu^+ \nu,\ D^0 \to K\pi$. Systematic error from our selection requirements was investigated by comparing a large number of kinematic quantities between data and MC simulation, and we generally found very good, although not perfect agreement. These differences do introduce systematic error, but in most cases, the small systematic cancels since only the efficiency ratio is relevant. A source of systematic error is the $\sim$15% better IP resolution in simulation compared to data, which leads to an underestimate of the efficiency of the IP χ^2 cuts from MC simulation. The worse resolution in data effectively means a looser IP χ^2 cut relative to simulation. This systematic has been evaluated by re-running the $X_b \to X_c\pi^-\pi^+\pi^-$ selection on the signal MC with the IP $\chi^2 > 9$ cut reduced to 6.25 (2.5σ), and measuring the increase in signal efficiency. We apply a correction equal to the increase in efficiency, and assign a 50% uncertainty on its value, resulting in a correction to the ratio of branching fractions of 0.970 ± 0.015. In addition to the IP χ^2 cuts, worse resolution in data implies the vertex χ^2/dof is slightly broader in data as compared to simulation. We find the simulation underestimates the efficiency loss from the vertex χ^2 cuts, leading to a correction on the ratio of branching fractions of 1.050 ± 0.025.

Another difference between the $X_b \to X_c\pi^-$ and $X_b \to X_c\pi^-\pi^+\pi^-$ selection is the differing selections on the number of long tracks, and the larger PV multiplicities in data compared to simulation. We use the $\bar{B}^0 \to D^+\pi^-$ sample, whose cut is at 180 long tracks, to assess the loss in $B^- \to D^0\pi^-$ and $\Lambda_b^0 \to \Lambda_c^+\pi^-$, where the cut is at 120. We then use the $\bar{B}^0 \to D^+\pi^-\pi^+\pi^-$ (cut at 300 long tracks) to assess the loss in $\bar{B}^0 \to D^+\pi^-$ from the cut at 180 long tracks. The corrections are found to be 0.99 ± 0.01 for the $\bar{B}^0$ and $\bar{B}_s^0$ branching fraction ratios, and 0.945 ± 0.010 for the B^- and Λ_b^0 ratios.

Another possible difference between data and simulation is the inefficiency due to the p_T cuts on the B, D and $\pi\pi\pi$ system. We estimate this by comparing data and signal MC, assuming a linear decrease of the rate from the cut value to zero. We find agreement to within 1%, which we assign as a systematic error.

We have also considered the uncertainty due to the underlying sub-processes that contribute to the $\pi\pi\pi$ final state. We find that the efficiency is flat across the full $M(\pi\pi\pi)$ range from 0.8-3.0 GeV/c^2, however, this is only one projection of the final state. The most significant drop in efficiency typically results for decays of the type $X_b \to X_c^*\pi$, or $X_b \to X_c^*\pi\pi$, where the excited charmed hadron X_c^* decays to $X_c\pi\pi$, or $X_c\pi$. The Q value in these decays is small, and this results in relatively soft pions, which have lower detection efficiency. For B^- ($\bar{B}^0$), the known contribution from the intermediate $D_1(2420)$ state is $\sim$ 5% ($\sim 1-2\%$) of the total rate, and thus is quite small, and is simulated. We have searched for the $\bar{B}_s^0 \to D_{s1}(2460)^+\pi^- \to D_s^+\pi^-\pi^+\pi^-$, via the mass difference, $M(D_s\pi\pi) - M(D_s)$, but find no evidence within the available statistics. Regarding the Λ_b^0, CDF has reported preliminary results on excited charmed baryons in the $\Lambda_b^0 \to \Lambda_c^+\pi^-\pi^+\pi^-$ decay [15], and they find about 9% of the total rate passes through either the $\Lambda_c(2595)^+$ or $\Lambda_c(2625)^+$, and about 14% through Σ_c^0 or Σ_c^{++}. We have checked that our data are consistent with the CDF results within (large) uncertainties. Our $\Lambda_b^0 \to \Lambda_c^+\pi^-\pi^+\pi^-$ signal MC does include the intermediate excited Λ_c states, at a larger fraction than observed in

the CDF data, but not the intermediate Σ_c contributions. The two factors offset, and we estimate this introduces a 3% systematic error on the Λ_b^0 efficiency from our simulation.

Particle identification requirements also contribute to the uncertainty. The PID efficiency is measured using calibration samples that include tagged $D^{*+} \to \pi^+ D^0$, $K_S^0 \to \pi^+\pi^-$, and $\Lambda \to p\pi^-$ decays. The PID likelihood distributions from these calibration samples are weighted to properly match the p, p_T, η distribution of the signal tracks, as well as the number of charged tracks in the signal events. After this re-weighting, we find that the simulation overestimates the PID efficiency by about 0.6%, we thus apply a correction of 1.01 ± 0.01, where we have conservatively taken a 1% uncertainty on the overall PID efficiency ratio determination.

Additional uncertainty may arise in estimating the ratio of L0 trigger efficiencies, which may depend on the underlying p_T spectrum of the b-hadrons, or on an imperfect simulation of the energy response of the calorimeters. To first order, we expect these differences to cancel in the ratio. To test this assumption, we re-weight the b-hadron p_T spectra to introduce decrease (increase) the number of b hadrons at low (large) p_T relative to its nominal shape. After re-weighting, we find that the average trigger efficiency of all decay modes increases by about 20%, but all trigger efficiency ratios are unchanged at the level of $\pm 1\%$. Based on this insensitivity to a dramatic change in the p_T spectrum of the signal B, or equivalently, the calorimeter energy response, we conservatively assign a 5% uncertainty to the ratio of L0 trigger efficiencies. The HLT1 and HLT2 efficiencies are in the 80-90% range, and we use the same triggers for both the $X_b \to X_c\pi^-\pi^+\pi^-$ and $X_b \to X_c\pi^-$ decay modes. We thus expect a very high degree of cancellation of systematic errors. We believe 2% to be a reasonable estimate of the possible systematic error on the ratio of HLT trigger efficiencies.

Fitting systematics are evaluated by varying the background shapes for both the $X_b \to X_c\pi^-\pi^+\pi^-$ and $X_b \to X_c\pi^-$ modes and re-measuring the yield ratios. Beyond our exponential, we have also tried first and second order polynomials. We find the ratios vary by up to 3% as we vary the background shape. We have also relaxed the various background constraints used in the fit, and find the ratio of yields varies by about 1%, except for $\bar{B}_s^0 \to D_s^+\pi^-\pi^+\pi^-$ and $\bar{B}_s^0 \to D_s^+\pi^-$, where we find deviations as large as 5% when varying the constraint on the $\bar{B}^0 \to D^+\pi^-\pi^+\pi^-$ and $\bar{B}^0 \to D^+\pi^-$ reflections. For the signal model, our default PDF is a double Gaussian, where the the narrow Gaussian fractional area and the ratio of the wider to narrower Gaussian are constrained to the values from simulation (with a relative error of $\approx$10%). To assess our sensitivity to the central values of these constraints, they are increased and decreased by 10% (relative) one at a time, for both the signal and normalization mode. The resulting deviations in the relative yields are generally small, and when added in quadrature, total 2%. We also include a systematic uncertainty of 1% for neglecting the small radiative tail in the fit. Taken together, we assign a 4% uncertainty to the relative yields from fitting, except for the B_s^0 ratio, where we assign 6.4%.

Another difference between data and MC simulation is related to multiple candidates. In the signal MC, we obtain the efficiency using reconstructed decays that match to a true signal decay, whereas in data, we choose only one candidate per event. Because

the multiple candidate rate is below 10%, and when there are multiple candidates, the correct candidate is chosen $(75 \pm 20)\%$ of the time, the correction is no larger than 2.5% (see Table 5 for precise values.) We ascribe a 50% relative uncertainty to the correction.

Lastly, we have comparable MC statistics in all our samples, from which we incur about 4% uncertainty. The various corrections and systematic uncertainties are listed in Table 5.

Table 5: Summary of corrections and systematic uncertainties to the ratio of branching fractions $\mathcal{B}(X_b \to X_c\pi^-\pi^+\pi^-)/\mathcal{B}(X_b \to X_c\pi^-)$, for $X_b = \bar{B}^0$, B^-, $\bar{B}^0_s$, and Λ^0_b. Note that numbers have been rounded to the second decimal place.

Quantity	central value $\pm$ syst. error			
	$\bar{B}^0$	B^-	$\bar{B}^0_s$	Λ^0_b
Track reconstruction	1.00 ± 0.06			
IP χ^2 cuts	0.97 ± 0.02			
Vertex reconstruction	1.05 ± 0.03			
Number of long tracks	0.99 ± 0.01	0.95 ± 0.01	0.99 ± 0.01	0.95 ± 0.01
p_T of D meson	1.00 ± 0.01			
$\Lambda^0_b \to \Lambda^+_c\pi^-\pi^+\pi^-$ substructure	1.00	1.00	1.00	1.00 ± 0.03
PID	1.01 ± 0.01			
L0 Efficiency	1.00 ± 0.05			
HLT Efficiency	1.00 ± 0.02			
Fitting	1.00 ± 0.04	1.00 ± 0.04	1.00 ± 0.064	1.00 ± 0.04
Multiple candidates	1.02 ± 0.01	1.01 ± 0.01	1.02 ± 0.01	1.03 ± 0.02
MC statistics	1.00 ± 0.04	1.00 ± 0.03	1.00 ± 0.05	1.00 ± 0.04
Total correction	1.03	0.98	1.04	1.00
Total systematic (%)	10.1	9.8	11.4	10.5

9 Final Results and Summary

Our final results for the ratio of branching fractions are:

$$\frac{\mathcal{B}(\bar{B}^0 \to D^+\pi^-\pi^+\pi^-)}{\mathcal{B}(\bar{B}^0 \to D^+\pi^-)} = 2.35 \pm 0.11(\text{stat}) \pm 0.24(\text{syst})$$
$$\frac{\mathcal{B}(B^- \to D^0\pi^-\pi^+\pi^-)}{\mathcal{B}(B^- \to D^0\pi^-)} = 1.26 \pm 0.07(\text{stat}) \pm 0.12(\text{syst})$$
$$\frac{\mathcal{B}(\bar{B}_s^0 \to D_s^+\pi^-\pi^+\pi^-)}{\mathcal{B}(\bar{B}_s^0 \to D_s^+\pi^-)} = 2.22 \pm 0.41(\text{stat}) \pm 0.25(\text{syst})$$
$$\frac{\mathcal{B}(\Lambda_b^0 \to \Lambda_c^+\pi^-\pi^+\pi^-)}{\mathcal{B}(\Lambda_b^0 \to \Lambda_c^+\pi^-)} = 1.32 \pm 0.15(\text{stat}) \pm 0.14(\text{syst})$$

If we use the world average values for the $X_b \to X_c\pi^-$ decays (see Table 1), we obtain the following branching fractions:

$$\mathcal{B}(\bar{B}^0 \to D^+\pi^-\pi^+\pi^-) = (6.16 \pm 0.26(\text{stat}) \pm 0.69(\text{syst})) \times 10^{-3}$$
$$\mathcal{B}(B^- \to D^0\pi^-\pi^+\pi^-) = (5.96 \pm 0.29(\text{stat}) \pm 0.61(\text{syst})) \times 10^{-3}$$
$$\mathcal{B}(\bar{B}_s^0 \to D_s^+\pi^-\pi^+\pi^-) = (6.28 \pm 1.10(\text{stat}) \pm 1.21(\text{syst})) \times 10^{-3}$$
$$\mathcal{B}(\Lambda_b^0 \to \Lambda_c^+\pi^-\pi^+\pi^-) = (12.2 \pm 1.4(\text{stat}) \pm 4.6(\text{syst})) \times 10^{-3}$$

These measurements are all substantially more precise than the current world average values. The $\Lambda_b^0 \to \Lambda_c^+\pi^-\pi^+\pi^-$ measurement is the first measurement of this decay breanching fraction. While its absolute branching fraction uncertainty is dominated by the uncertainty in the $\Lambda_c \to pK\pi$ branching ratio, the branching fraction ratio given above is insensitive to this uncertainty. It is interesting to note that while the $B^- \to D^0\pi^-$ amplitude is about 35% larger than the one in $\bar{B}^0 \to D^+\pi^-$, this increase is not evident when the $\bar{u}d$ produces a $\pi\pi\pi$ state. In terms of Feynman diagrams, this may imply a smaller contribution from the color-suppressed diagram in $B^- \to D^0\pi^-\pi^+\pi^-$ compared to $B^- \to D^0\pi^-$, or a different relative strong phase, relative to the external tree diagram [16].

In summary, we have performed new measurements of the branching fractions of the Cabibbo-favoured decays $X_b \to X_c\pi^-\pi^+\pi^-$ relative to $X_b \to X_c\pi^-$ and these measurements provide the most precise determinations of their rates. We find that the rates for the $\pi\pi\pi$ bachelor final states are at least as large or even twice as large as the single-π bachelor states. These larger rates could make them very useful for CP violation studies, where they play an analogous role to the single-π bachelor final state.

References

[1] N. Cabibbo, Phys. Rev. Lett. **10**, 531 (1963); M. Kobayashi and T. Maskawa, Prog. Theor. Phys. **49**, 652 (1973).

[2] D. Atwood, I Dunietz and A. Soni, Phys. Rev. Lett **78**, 3257 (1997); Phys. Rev. D **63**, 036005 (2001).

[3] M. Gronau and D. Wyler, Phys. Lett. B **265**, 172 (1991); M. Gronau and D. London, Phys .Lett. B **253**, 483 (1991).

[4] A. Giri, Y. Grossman, A. Soffer and J. Zupan, Phys. Rev. D **68** 054018 (2003).

[5] P. del Amo Sanchez *et. al.* (BaBar Collaboration), Phys. Rev. D **82**, 072004 (2010); P. del Amo Sanchez *et. al.* (BaBar Collaboration), Phys. Rev. Lett **105**, 121801 (2010).

[6] A. Poluektov *et. al.* (Belle Collaboration), Phys. Rev. D **81**, 112002 (2010).

[7] K. Nakamura *et al.,* J. Phys. G 37 075021 (2010).

[8] A. A. Alves Jr. *et al.* [LHCb Collaboration], JINST 3, S08005 (2008).

[9] V. Gligorov, *"A single track HLT1 trigger"*, LHCb-PUB-2011-003.

[10] M. Willims, *et. al.*, *"The HLT2 Topological Lines"*, LHCb-PUB-2011-002.

[11] T. Sjöstrand, S. Mrenna and P. Skands, JHEP 0605, 026 (2006).

[12] A. Ryd *et al.,* "EvtGen: a Monte Carlo generator for B-physics", BaBar Analysis Document 522 (2005); D. J. Lange, Nucl. Instrum. Meth. A **462**, 152 (2001).

[13] S. Agostinelli *et al.* [GEANT4 Collaboration], Nucl. Instrum. Meth. A **506**, 250 (2003).

[14] R. Aaij *et. al.* (LHCb Collaboration), Phys. Lett. B **694**, 209 (2010).

[15] See `http://www-cdf.fnal.gov/physics/new/bottom/091029.blessed-Lb2Lc3pi-structure/LbLc3pi.html`.

[16] Cheng-Wei Chang and J. Rosner, Phys. Rev. F **67** 074013 (2003); C. S. Kim *et al* , Phys. Lett B **621** 259-268 (2004).